GEOLOGICA CARPATHICA, FEBRUARY 2020, 71, 1, 47–60 https://doi.org/10.31577/GeolCarp.71.1.4

Delineating the subsurface geological features of the Southern Abu Gharadig Basin, North Western Desert, Egypt, based on gravity and magnetic data

SAADA AHMED SAADA✉

Faculty of Science, Geology Department, Suez University, Suez, Egypt; ✉saada.elsayed@suezuniv.edu.eg

(Manuscript received December 28, 2018; accepted in revised form December 16, 2019)

Abstract: The gravity and magnetic data in the area south of the Qattara Depression has been investigated to define the structural framework of that area. Several techniques were applied to these data such as separation of regional and residual components, lineament analysis, tilt angle derivative, spectral analysis, and 2.5D gravity and magnetic modelling. The regional-residual separation was carried out using the Fast Fourier Transform to assess the sedimentary basins and the uplifted blocks. Lineament analysis was carried out to explain the main tectonic trends. The spectral analysis technique was applied to magnetic data to determine the depth to the basement surface along 21 profiles. 2.5D gravity and magnetic modelling along four profiles indicates that the area is formed from uplifted and down-faulted blocks of granitic and basaltic rocks. A tentative structural relief map was constructed to outline the main basins and uplifts. The results of this study show a thick sedimentary cover within the Abu Gharadig Basin exceeds 3000 m in most parts of the area under consideration. This sedimentary cover is thin in the south-western part within Faghur Basin. The structural pattern indicates that the area was affected mainly by: NE (Tibesti), ENE (Syrian Arc), N–S (East African), and NW (Suez) tectonic trends. The geothermal gradient was determined for six square areas. It has an average value of about 20.23 °C/km that can generate hydrocarbons within the outlined sedimentary basins. Because of the presence of thick clastic to carbonate rocks that were subjected to faulting and sufficient geothermal gradient to mature source rock; the Southern Faghur and Abu Gharadig basins can be considered as a promising region for further hydrocarbon exploration.

Keywords: Qattara Depression, FFT, 2.5D-modelling, tilt angle derivative, structure map, gravity and magnetic data.

Introduction

The interpretation of the potential field data is a very essential step for mapping and exploration purposes. Generally, it is the first step in both petroleum and mineral explorations. Such phases give us an idea about the subsurface distribution of the underlying gravity and/or magnetic sources. The aeromagnetic survey is used for defining the depth of magnetic sources of an anomaly above any region employs the belief that the magnetic field measured at the earth's surface comes from different depths (shallower than the Curie point depth). The first step after removing the diurnal variations is removing the Earth's main field and residual magnetic data is related to the crustal field, which depends mainly on the magnetic susceptibilities and/or the structures of the basement rocks. The spectral analysis was employed to assess the middling depth to basement rocks (sedimentary thickness) across the geological area. On the other hand, gravity survey informs us about the subsurface distribution of the densities that can result from uplifted and down-faulted blocks and/or the mineralogical changes.

The Western Desert (WD) is the second most encouraging area of hydrocarbon prospective after the Gulf of Suez province. It covers two-thirds of the land surface of Egypt (about 680,650 square km) of an intracratonic basin in an unstable shelf region where the basinal areas are widespread. The WD is a huge platform with a mean elevation of 500 m above sea level consisting of thick-layered sedimentary rocks largely unaffected by tectonic disturbances (Said 1990). The northern part of the WD has many prospective sedimentary rocks, ranging in age from Paleozoic to Tertiary, in four main basins: Abu Gharadig, Alamein, Matruh-Shushan, and Faghur (Shahin 1989).

Most oil discoveries are concentrated north of Latitude 29°N, where several investigations were applied, for example by El-Khadragy et al. (2010); Shahin & Al-Awadly (2011), Abu El-Ata et al. (2012); Shaaban et al. (2012); Azab (2014), Mohamed et al. (2016). Only a few papers were researched south of this latitude, which focuses on the oases of the WD such as El-Badrawy & Soliman (2003); Abdel Zaher et al. (2009); Saada & El-Khadragy (2015). In this work, the author tries to throw more light on: (1) The structural framework of the area south of the Qattara Depression by utilizing the potential field (gravity and magnetic) data; (2) The fault pattern and main trends that affected the study area; (3) The nature of the magnetic sources within the area under investigation; (4) The geothermal gradient (GG) within the area that helps to generate hydrocarbons.

The study area

The research area lies to the south of the Qattara Depression. It extends between latitudes 27°30'–29° 00'N and longitudes

26°00'–28°00'E (Fig. 1). The surface area of this region is about 31,700 square km. The outcrops of this area are mostly composed of rocks and sediments going back to the Eocene, recent sand dunes of Quaternary ages with a few outcrops of Miocene and Oligocene. The Eocene deposits (Te) are composed mainly of the thick marine limestone with chert and minor clay beds. Oligocene outcrops (To) are denoted by both fluvial and/or lacustrine clastics and gravel pieces. Miocene deposits (Tm) are not observed in the area as fine and coarse clastic rocks (Fig. 1). Undivided Quaternary deposits (Q), mainly alluvial deposits of sand and gravel, outcrop in the middle part as disseminated locations. Moreover, sand dunes

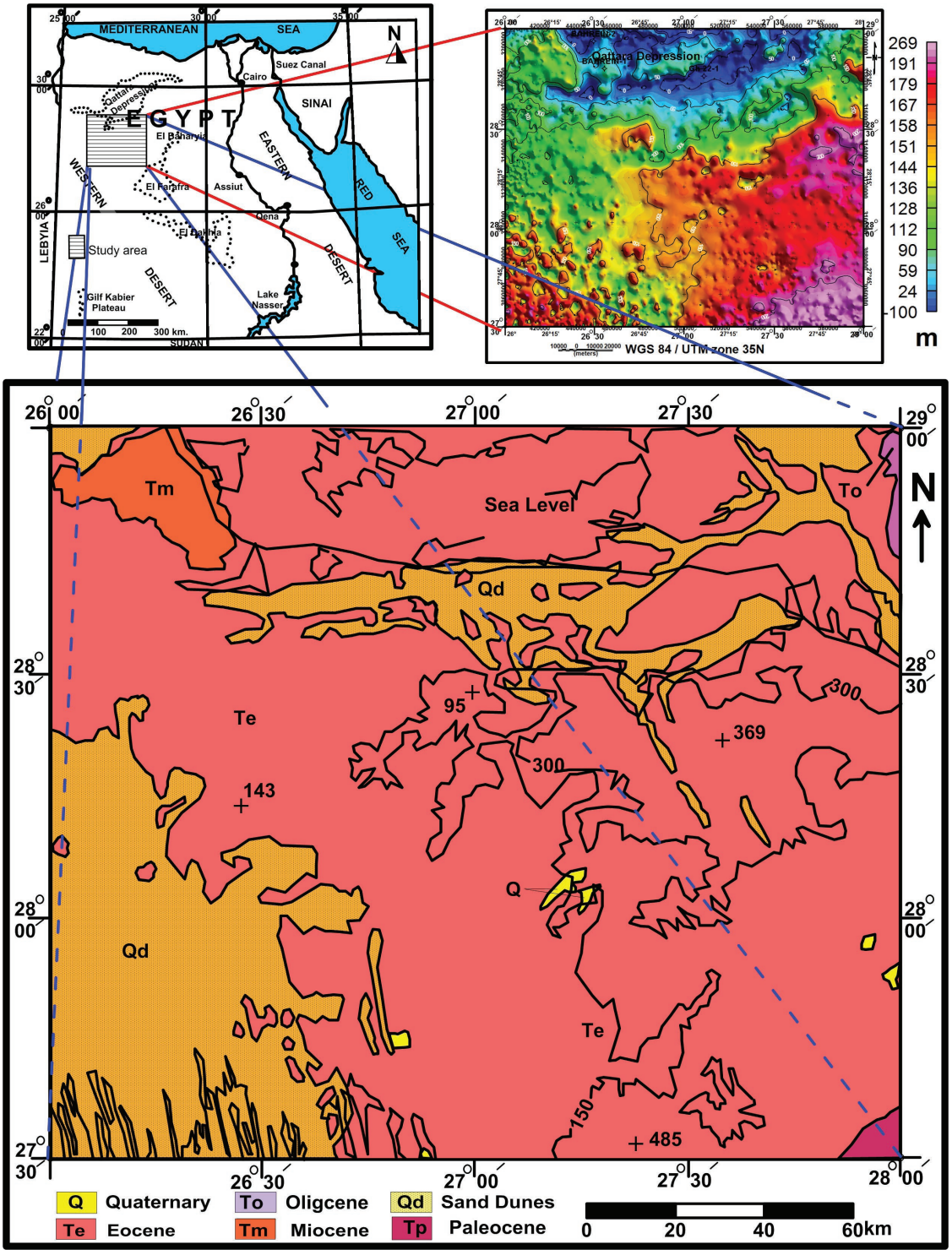

Fig. 1. Location map shows the topographic and geological maps (Egyptian Geological Survey and Mining Authority 1981).

(Qd) generally run in a NNW direction and represent the Pliocene–Recent, especially in the south-western and northern parts of the investigated area.

Topographically, the area under investigation shows an irregular surface with dissimilar ages as explained above. The northern part characterized by the presence of the Qattara Depression with a minimum elevation within the study area attains about −100 m below the sea level. Conversely, the south-eastern corner has a maximum elevation of the ground surface reaching 269 m. The surface of the south-western area composed mainly of sand dunes with elevations range from 100–200 m of the Great Sand Sea.

General geology and tectonics

The WD involves three main tectonic provinces that controlled its stratigraphic and structural pattern. These are: (1) the Arabian-Nubian massif, which is represented by its red colour and is exposed in the Owienat, Eastern Desert and South Sinai; (2) The stable shelf covers a large part of Egypt surrounding the Craton Nubian massif. It reflects relative tectonic stability towards the south. (3) The unstable shelf that underwent many intense rock distortions and includes the northern part of the WD (Youssef 2003).

Structurally, the area lies mainly within the unstable mobile belt of the tectonic framework of the Egyptian Territory (Said 1962). Accordingly, near and rough basement rocks can be distinguished. The stratigraphic system is described by asymmetric linear folding, and faulting in many portions. The examined area has suffered different tectonic events from the Pre-Cambrian period to Recent. The Pre-Cambrian tectonic trends include East African (N–S), Suez (NNW) and Tibesti (NE) trends, which are preserved in the basement rocks of the northern WD (Meshref 1990, 1995). Younger tectonic trends appeared during the Paleozoic era and resulted from thrusting of the Africa continent due to its moving northward against the main block of the earth`s crust that causes the formation of the E–W trend. This trend is revealed in the northern WD in Regional magnetic and isopach maps (Meshref 1990). In addition, the E–W (Mediterranean) trend is exposed in many parts of Middle-Upper Jurassic formations (Meshref 1990). Younger tectonism in the Late Jurassic to Early Tertiary was caused by activities of Africa in relation to Laurasia (Tethyan plate movement). These activities act in two stages (Sultan & Abdel Halim 1988; Hantar 1990; Meshref 1990): (1) The Sinistral shear displacements through the Late Jurassic to Early Cretaceous (Nevadian orogeny). The E–W faults and the NW fold resulted. They linked thrust faults and ENE strike-slip faults (Dolson et al. 2001). (2) The Dextral shear movements, which occurred at the end of the Cretaceous to the beginning of the Tertiary (Laramide movement). Therefore, two tectonic features were recorded with wrench chief E–W faults, ENE fold (Syrian arc system) trend, which linked with the thrust faults and WNW (Najd) strike-slip faults. After these movements, the African plate moved toward the Laurasian one (the Alpine orogeny). The N–S and the NNW–SSE trend were formed by this movement (Youssef 1968; Dietz & Hoden 1970). Many researchers (e.g., Said 1962; Abu El-Ata 1981, 1988; Meshref 1982, 1990, 2002; Dennis 1984; Abdel Aal & Moustafa 1988; Sultan & Abdel Halim 1988; El-Kenawy 2000; Azab 2014; Saada & El-Khadragy 2015 and others) have worked and are still working on the WD structures.

Stratigraphically, the investigated area exhibits rocks ranging in age from Cambrian to Recent, as shown from the three drilled wells (Bahrein-1, 2 and Gh 22-1). Barakat (1984) divided the wholly sedimentary sequence of the northern WD into: (1) the lower clastic section (ranges from Cambrian to Early Mesozoic); (2) the middle calcareous section (from Cenomanian to Late Eocene); and (3) the upper clastic section (ranges in age from Oligocene to Recent). The generalized stratigraphic column of the northern WD (Fig. 2) shows that the subsurface stratigraphic sequence ranges in age from Cambro–Ordovician to Recent (recorded in Bahrein-1 well), resting unconformably over the crystalline basement rocks (Shaarawy 1994).

Data and methodology

This study is based mainly on the potential field data that include the Bouguer and the Reduced to Pole (RTP) aeromagnetic maps. The Bouguer anomaly map was collected by the General Petroleum Company (GPC 1984) of Egypt with a scale of 1:200,000 and a station interval of 1 km as well as a line spacing of 5 km. The contour interval of this map is 1 mGal. The standard values of 0.3086 mGal/m and 2670 kg/m^3 were used for the Free-Air and the Bouguer corrections, respectively. The total intensity aeromagnetic map of the area had been surveyed and compiled by Compagnie Generale de Geophysique of Italian Egyptian Oil Company (IEOC) for the Egyptian General Petroleum Corporation (EGPC) dated in Nov–Dec 1994, with the scale of 1:250,000 and contour interval of 2 nT, aircraft and altitude 610 m. The inclination angle of the area ranges between 39°–41°N, and the declination angle is about 0.25°E. These data were reduced to pole and published in El-Kenawy (2000). Three drilled wells (Table 1) were used to constrain the modelled profiles and stratigraphic section within the study area.

Analysis of potential field data

The Bouguer map (Fig. 3) shows that the area has a main negative anomaly with amplitude less than −40 mGal and trending in the NE direction. Another negative anomaly with a gravity minimum (attains about –49 mGals) is situated at the western corner. On the other hand, positive anomalies that can be interpreted as uplifted blocks outline these basins. The maximum positive anomaly lies around Bahrein-1 well with an amplitude of 4 mGal that may be related to high

density and/or uplifted blocks. Positive anomalies are trending in the NE, NS and NW directions. Linear anomalies denote faults reveal an NE trend.

Qualitatively, the RTP magnetic map (Fig. 4) of the study area reveals a series of positive and negative anomalies with different sizes, shapes, trends, and extensions, with nearly uniform or gentle gradients all over the area of interest. The trends of the anomalies are mostly in the N–S, ENE, and NW directions. The north-eastern anomaly has the minimum amplitude of −119 nT trending in the NE direction. On contrary, the maximum amplitude of 411 nT is shown in the northern part (profile P19). This high amplitude reflects the nature of magnetic sources.

Separation of regional and residual components

The measured potential anomaly at the earth's surface is not created by only one single structure but it is the sum of the effects of complex subsurface structures buried at different depths. The regional-residual separation process is used

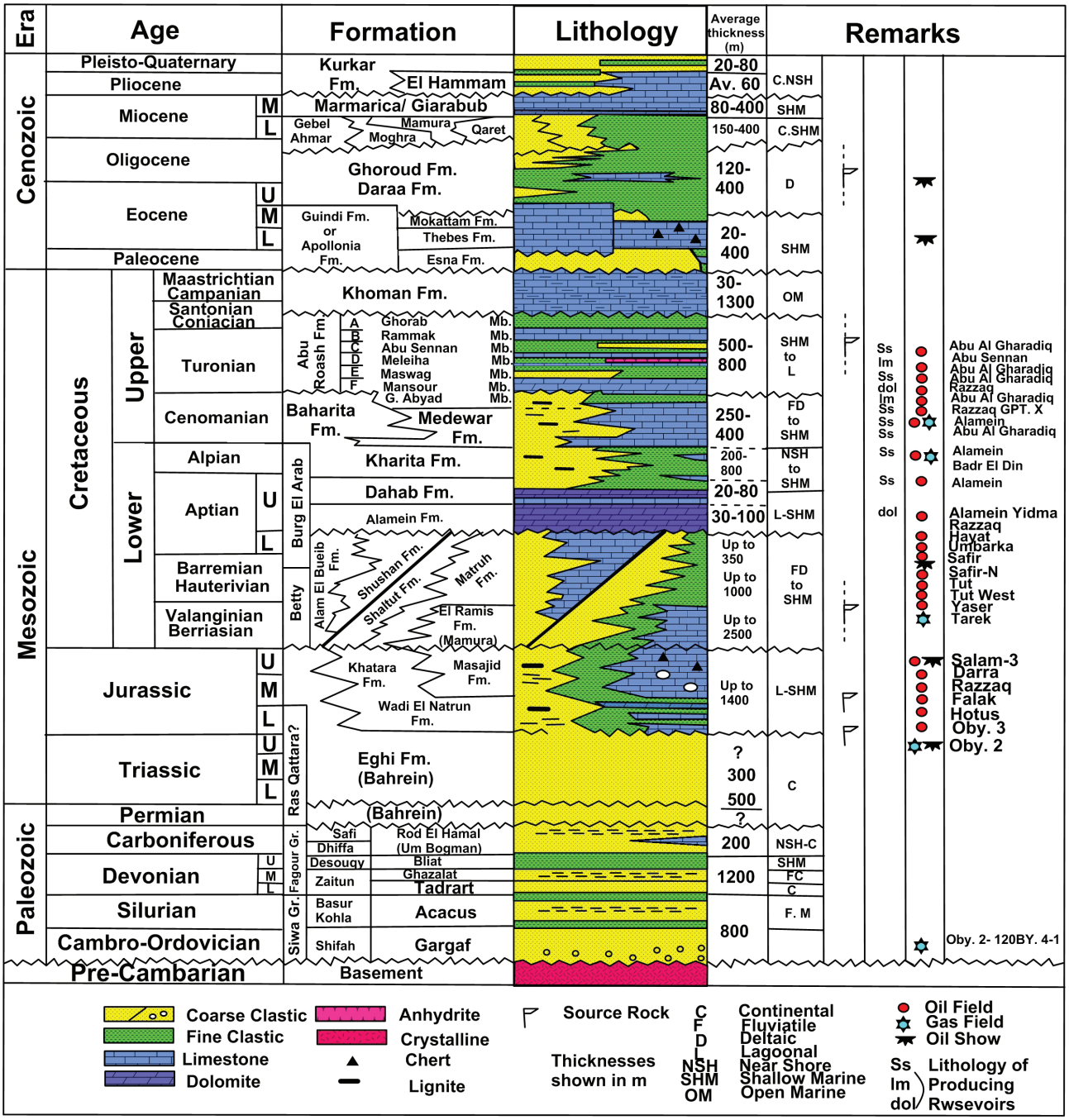

Fig. 2. The Stratigraphic Column of the WD (after BAPETCO 2007).

Table 1: The drilled well data.

Well name	Latitude	Longitude	Spud date	Complete date	Final total depth (m)	Formation total depth	Status/ remarks
BAHREIN-2	28°56'12.5"N	26°29'35.9"E	05/10/1970	02/11/1970	2145.4	Devonian	Dry well
BAHREIN-1	28°47'57.6"N	26°33'12.0"E	22/04/1970	18/07/1970	3036.9	Ordovician	Dry well
Gh 22-1	28°45'40.5"N	27°06'33.6"E	27/02/1995	03/04/1995	2231.3	Khatatba Fm.	Dry well

to isolate the anomalies caused by shallower geological features from those of deeper ones. Removing the regional field from the observed one; resulting in the residual field. Generally, the regional anomalies are considered broad and smoothed; they are associated with the deeper and larger structures, while the residual ones seem to be of sharp shapes and high-frequencies, which reflect the shallow bodies (Nettleton 1976; Thébault et al. 2010; Abu El-Ata et al. 2012; Maden et al. 2015). So, the residual anomalies can be defined as the deviations from the mean or regional surface. The residual fields are important for bringing into focus any shallow anomalous features, which are usually of primary interest in geological prospecting. Generally, different methods are used for removing the regional components and the residuals.

Analysis of the 2D-power spectrum of potential data is useful and a reliable tool to guess the ensemble depths to different gravity or magnetic prospects with different changes in the density or magnetic susceptibilities, respectively (Naidu 1970; Spector & Grant 1970; Reddi et al. 1988). The assessment of source parameters is performed on gridded gravity and/or magnetic data. Two advantages can be concluded. Initially, it eliminates errors produced by survey lines, which are not adapted perpendicularly to its strike. Next, it does not depend on the selected window nor the operator size. Furthermore, the grids of the yield quantities generated and processed to improve detail and offer structural data that otherwise cannot be marked. Selim & Aboud (2012) indicated that the spectra of gravity and/or magnetic anomalies contain two slices. The first in the low-frequency end, which is denoted by a straight line and signifies the deeper discontinuities (Moho and/or Conrad for gravity and the Curie depth for magnetic). The second part is in the high-frequency portion, which denotes the shallower sources (basement and/or intrusions).

The Fast Fourier Transform (FFT) is used to isolate the regional (low-pass) anomalies from the residual (high-pass) ones. Figure 5 displays the radial average power spectrum for both gravity (Fig. 5a) and magnetic (Fig. 5b) maps. The inspection of the resulted radially averaged log power spectrum shows that a lower wavenumber one (regional component), denoted by the dotted straight line, reflects the deep-seated bodies. Meanwhile, the higher wavenumber represents the shallow (red straight line) contribution (residual component). The interactive filter of Oasis Montaj (2007) is used to define the cut-off wavenumber (0.01 Rad/m). The Butterworth filter is applied to gravity and magnetic (G/M) data for calculating both regional and residual components. Consequently, two low-passes and two high-passes maps resulted.

Generally, the regional maps display the low wavenumber (long wavelength) anomalies that denote the deeper sources.

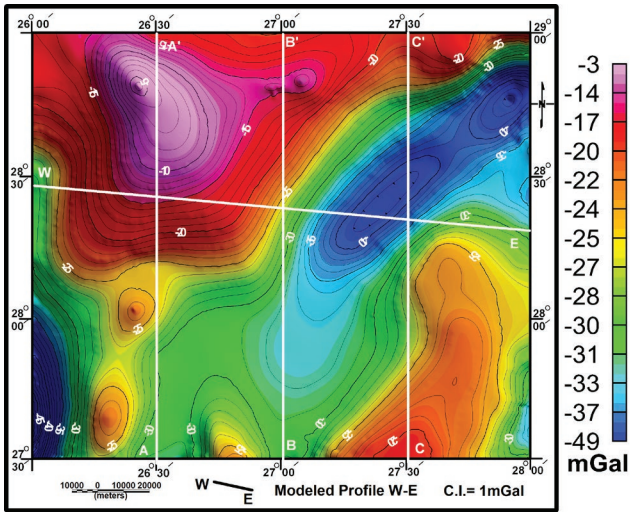

Fig. 3. The Bouguer gravity map of the research area (after GPC 1984) shows the locations of the gravity modelling profiles.

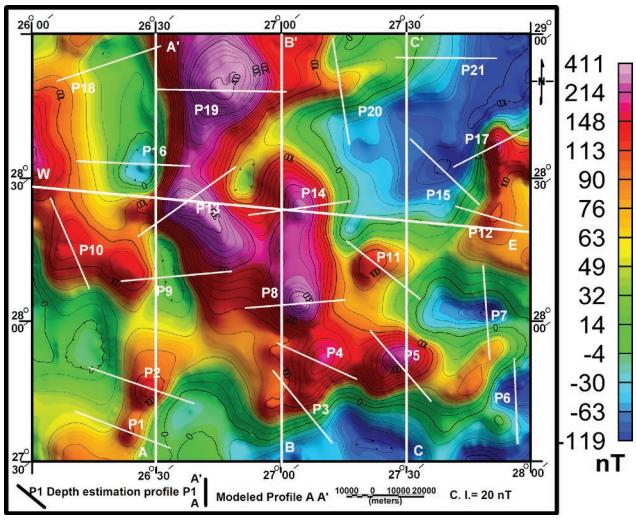

Fig. 4. The Reduced to Pole (RTP) magnetic map (after EGPC 1994) shows the locations of the spectral analysis and the 2.5D-magnetic modelling profiles.

Figure 6a shows the low-pass gravity map. It reveals a few numbers of closed gravity anomalies. Only two main negative anomalies that can be related to the southern Abu Gharadig and Faghur basins are displayed. The positive gravity anomalies may define the uplifted blocks that separate these two basins. The low-pass magnetic map (Fig. 6b) reflects the deep magnetic sources. The regional component of the RTP field

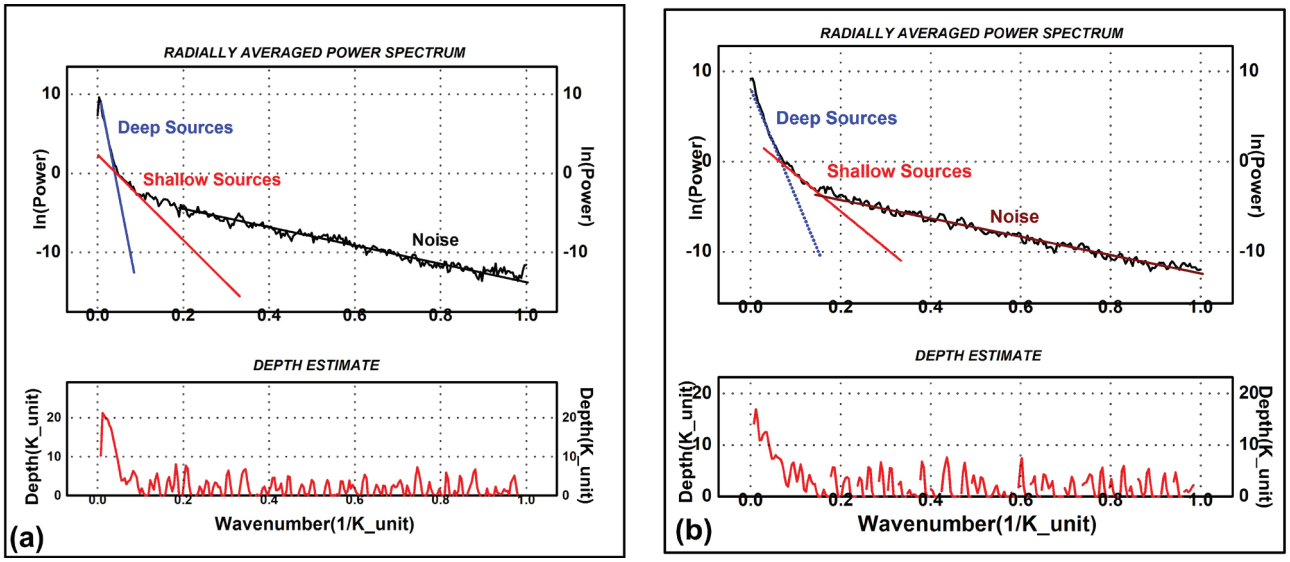

Fig. 5. Radially average power spectrum of both (**a**) gravity and (**b**) magnetic maps.

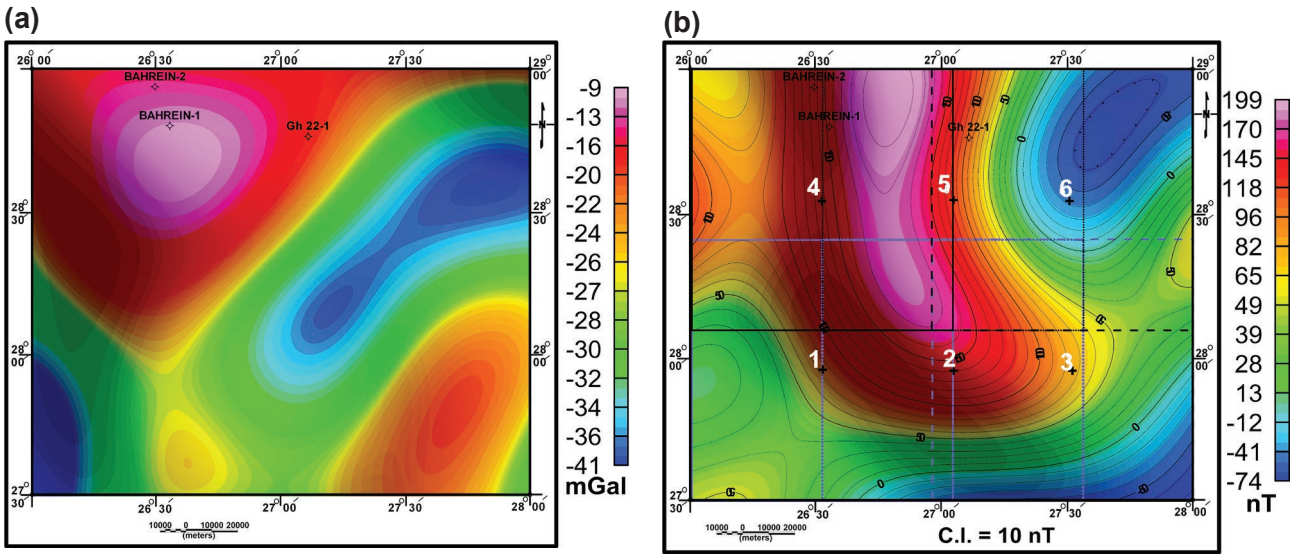

Fig. 6. a — The low-pass filtered gravity map with a cut-off wavenumber of 0.01 Rad/m. **b** — The low-pass filtered magnetic map with a cut-off wavenumber of 0.01 Rad/m shows the six blocks that were used to estimate the geothermal gradient.

indicates the deeper sources and hence support outlining of the possible magnetic layer within the crust (Rama Rao et al. 2011). Therefore, it is used as a base map to determine the bottom of the magnetic layer and the Curie isotherm, which will be discussed later. This figure reveals a good similarity as compared with Fig. 6a except for the southern part.

Both the residual (high-pass) gravity and magnetic (G/M) maps (Fig. 7a,b) show the distribution of G/M field after eliminating the regional effect. These maps are characterized by the dominance of various alternating local positive and negative anomalies of different sizes, shapes and orientations of relatively high-wavenumbers, weak amplitude and sharp gradients reflecting different causative G/M sources of shallow depth seated origin. However, the high-pass gravity map is characterized by several minor elongated anomalies distributed throughout the study area with amplitude ranges from −9.8 to 8.3 mGal. Due to the removal of the regional magnetic field, the residual RTP magnetic map is practically free of the profound crustal heterogeneities and shows the scattering of the several high and low susceptibility blocks, with amplitudes ranging between −152 and 235 nT. These high amplitudes indicate that the subsurface is intruded by many sources of high magnetic susceptibilities. From this filtration process, the most dominant trends in the study area are the N–S, NE, and E–W trends.

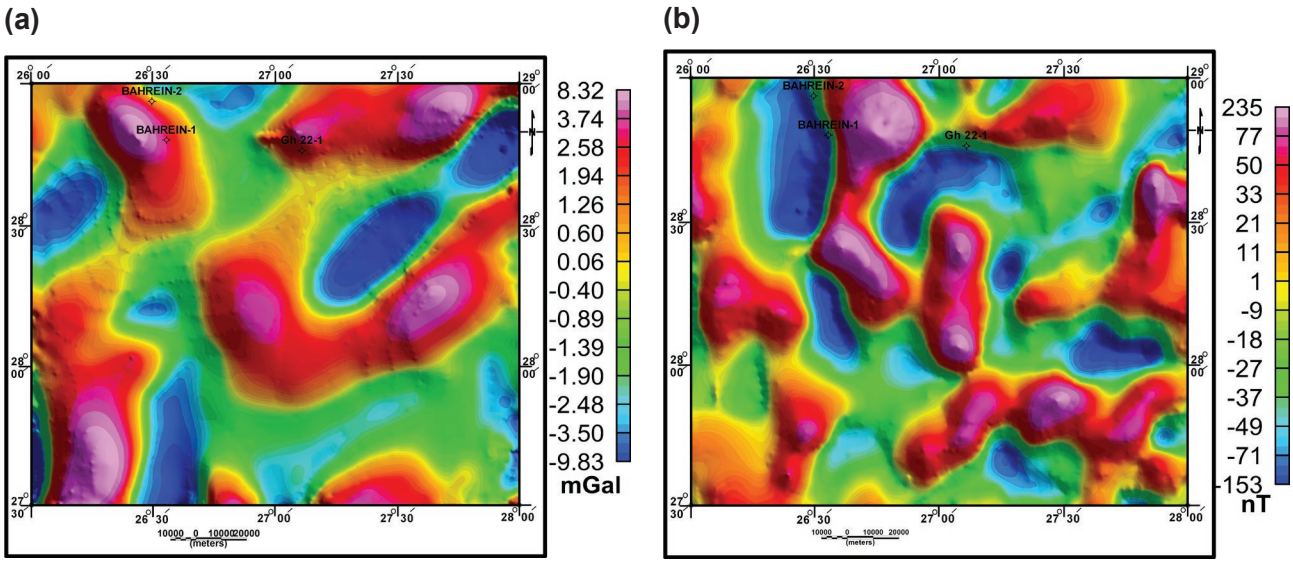

Fig. 7. a — The high-pass filtered gravity map with a cut-off wavenumber of 0.01 Rad/m. **b** — The high-pass filtered magnetic map with a cut-off wavenumber of 0.01 Rad/m.

Structural trend analysis

G/M data are normally used for mapping and delineating contacts between rocks with different physical properties and such contact regularly occurs along fault boundaries. In oil exploration, for instance, G/M data are used for identifying faults of the basement rocks, which may control the developments and depositional history of the sedimentary basins. In general, these G/M anomalies align themselves along structural trends. It has been shown that gravity/magnetic trend patterns usually delineate provinces, which in turn reveal the subsurface tectonics (Affleck 1963). The purpose of the lineament analysis is to determine statistically the main tectonic trends, which affected the basement rocks and the overlying sedimentary section of this area (El-Gezeery 2006).

According to Affleck (1963) technique and the first horizontal gradient, the structural trends and the major faults were determined for both G/M data. The interpreted trends from gravity (Bouguer, regional and residual) maps and magnetic (RTP, regional and residual) data show different trends affecting the study area. These trends reflect the compressional and tensional forces that were active during different geological periods. The G/M trends exhibit a good correlation between the observed, regional and residual trends (or faults) with few exceptions for the residual trends that occasionally show different trends. These trends and faults were numbered and lengthen every 10° clockwise and anticlockwise from the North. Accordingly, the number and the length percentage, as well as the ratio of the length to the number, are calculated and summarized in Tables 2–7. The results of these statistical studies are plotted in the frequency curve (Fig. 8). It illustrates that the NE (Tibesti) trend is the major trend in the gravity maps as shown by the blue, purple and green colours as well as the regional magnetic map (purple color). This trend is represented in the western and north-western parts of the WD. The plot also displays that the area was affected by different tectonic trends such as the N–S (East African), ENE (Syrian Arc), NW (Suez), and NNE (Aqaba) trends.

The tilt angle derivative (TDR)

The TDR is applied to potential data to map shallow basement structures, explore mineral targets and determine the edges of the causative bodies (Geosoft Oasis Montaj 2007). Miller & Singh (1994) and Verduzco et al. (2004) proposed the tilt angle filter. It was advanced by many authors such as Salem et al. (2007, 2008) and Fairhead et al. (2008). It presented a significant attention due to its essential and applied simplicity (Hinze et al. 2013). The TDR is calculated by computing the Arctan of the vertical to the horizontal derivatives. So, the output ranges from $-\pi/2$ to $+\pi/2$ (radian). Half of the horizontal distance between $-\pi/4$ (-0.785) and $+\pi/4$ ($+0.785$) determines the depth to contact. Generally, the zero line defines the location of the edge/contact. Positive values lie above uplifted blocks whereas negative values refer to down-faulted ones. In this work, the TDR was applied to the high-pass gravity (because the Bouguer shows long wavenumbers that may be related mainly to deep sources) and the RTP data.

The TDR gravity map (Fig. 9a) outlines the edges/contacts of the uplifted blocks all over the study area. It displays alternative uplifted and down-faulted blocks. The depth to these edges/contacts ranges from 2–5km as shown from the half distance between the dotted yellow (with contour value of -0.785) and blue lines (contour value of $+0.785$).

The TDR magnetic map (Fig. 9b) reveals dissimilar edges as compared with the gravity map. The outlined edges of the causative bodies reflect different sizes, shapes, and trends. The depth to these edges seems to be shallower than that of the gravity maps. It ranges from about 1 to 3 km in most parts.

Estimating the average depths

The spectral analysis technique was used to calculate the depth to the basement surface along twenty-one magnetic profiles. The method was proposed by many authors for the investigating the potential field data. It calculates the depth to a number of bodies, such as the thin sheets that were examined by Troshkov & Shalaev (1961) and rectangular prismatic bodies that were introduced by Spector & Grant (1970) as well as the groups of thin sheets that were argued by Curtis and Jain (1975). According to the procedures of Spector & Grant (1970), the power spectrum may be single or double bands, where the later consists of two parts. The first, which relates to the deeper sources meaning basement depth that is represented by small wavenumbers and decreases rapidly. The second that arises from the shallower ensemble of sources namely intrusion ridges, denotes the higher wavenumber end of the spectrum.

The depths to the basement sources within the study area were considered using the spectral analysis technique along 21 magnetic profiles. The positions of the selected profiles (P1–P21) are displayed in Fig. 4. Figure 10 shows two examples along profiles P1 and P9 and the results of the depth estimation are shown in Table 8. The deep depth of the basement surface ranges from 2323 m (P1 in the south-western corner) and 4454 m (P9). The depth to the intruded bodies varies from 813 m (P12) to 1873 m (P15).

Table 2: The faults and trends parameters as shown by the Bouguer gravity map.

WEST					Azimuth	EAST				
N	N%	L(m)	L%	L/N		L/N	L%	L(m)	N%	N
1.0	3.6	41395.0	4.2	41395.0	0:<10	25916.5	7.8	77749.6	10.7	3.0
1.0	3.6	54128.0	5.4	54128.0	10:<20	31916.4	12.8	127665.7	14.3	4.0
2.0	7.1	70704.5	7.1	35352.3	20:<30	16398.8	1.6	16398.8	3.6	1.0
1.0	3.6	26746.9	2.7	26746.9	30:<40	57096.6	5.7	57096.6	3.6	1.0
1.0	3.6	19298.8	1.9	19298.8	40:<50	50354.5	35.3	352481.5	25.0	7.0
2.0	7.1	64121.0	6.4	32060.5	50:<60	23082.9	2.3	23082.9	3.6	1.0
0.0	0.0	0.0	0.0	–	60:<70	18686.5	1.9	18686.5	3.6	1.0
0.0	0.0	0.0	0.0	–	70:<80	–	0.0	0.0	0.0	0.0
0.0	0.0	0.0	0.0	–	80:<90	23913.0	4.8	47826.1	7.1	2.0
8.0	28.6	276394.1	27.7		Sum		72.3	720987.6	71.4	20.0
∑n	28.0		∑L=997381.7 m			∑n%	100.0		∑L%	100.0

Table 3: The faults and trends parameters as shown by the regional gravity map.

WEST					Azimuth	EAST				
N	N%	L(m)	L%	L/N		L/N	L%	L(m)	N%	N
0.0	0.0	0.0	0.0	–	0:<10	31088.1	10.0	93264.3	15.0	3.0
1.0	5.0	37357.2	4.0	37357.2	10:<20	–	0.0	0.0	0.0	0.0
1.0	5.0	65100.3	7.0	65100.3	20:<30	50557.1	10.8	101114.2	10.0	2.0
0.0	0.0	0.0	0.0	–	30:<40	61345.7	13.1	122691.3	10.0	2.0
3.0	15.0	118610.0	12.7	39536.7	40:<50	64887.5	13.9	129775.1	10.0	2.0
0.0	0.0	0.0	0.0	–	50:<60	42955.8	9.2	85911.7	10.0	2.0
0.0	0.0	0.0	0.0	–	60:<70	50771.9	5.4	50771.9	5.0	1.0
0.0	0.0	0.0	0.0	–	70:<80	41926.2	4.5	41926.2	5.0	1.0
1.0	5.0	70582.8	7.5	70582.8	80:<90	18723.9	2.0	18723.9	5.0	1.0
6.0	30.0	291650.3	31.2		Sum		68.8	644178.6	70.0	14.0
∑n	20.0		∑L=935829.0 m			∑n%	100.0		∑L%	100.0

Table 4: The faults and trends parameters as shown by the residual gravity map.

WEST					Azimuth	EAST				
N	N%	L(m)	L%	L/N		L/N	L%	L(m)	N%	N
1.0	1.8	26872.0	1.8	26872.0	0:<10	109239.2	7.4	109239.2	7.1	1.0
4.0	7.1	74712.2	5.1	18678.1	10:<20	28547.3	3.9	57094.5	3.6	2.0
4.0	7.1	83424.2	5.6	20856.0	20:<30	6284.2	1.7	25136.8	1.8	4.0
5.0	8.9	114061.5	7.7	22812.3	30:<40	24341.9	8.2	121709.6	8.9	5.0
3.0	5.4	60706.8	4.1	20235.6	40:<50	115659.1	23.5	346977.3	16.1	3.0
1.0	1.8	35205.5	2.4	35205.5	50:<60	232283.8	15.7	232283.8	17.9	1.0
0.0	0.0	0.0	0.0	–	60:<70	35538.1	7.2	106614.4	5.4	3.0
0.0	0.0	0.0	0.0	–	70:<80	19321.5	1.3	19321.5	1.8	1.0
1.0	1.8	20124.7	1.4	20124.7	80:<90	22451.6	3.0	44903.3	3.6	1.0
19.0	33.9	415106.9	28.1		Sum		71.9	1063280.3	66.1	21.0
∑n	40.0		∑L=1478387.2 m			∑n%	100.0		∑L%	100.0

The forward modelling profiles

To study the nature of the basement structures and determine the thickness of the sedimentary cover, three models were constructed along profiles AA', BB' and CC' using the GM-SYS program of Oasis Montaj (2007). The profiles were taken on the Bouguer (Fig. 3) and RTP aeromagnetic (Fig. 4) maps covering the strong magnetic signatures. Three profiles extend from South to North and the fourth profile runs from West to East to highlight the configuration of the basement surface. Three wells (Table 1) were used to constrain the modelled profiles. The sedimentary cover was modelled as two upper and lower units with 2.34 and 2.54 gr/cc, respectively. Both upper and lower sediments have a zero magnetic susceptibility. The modelled sections were shown with 9 km depth. The modelled profiles reveal a good fit between the observed and calculated magnetic profiles.

Profile AA' runs in the western portion along Longitude 26°30'E, extending a distance of about 165km. It shows two basinal features of the south Faghur Basin in the middle and the northern parts. Figure 11 displays a good fitness between both the observed and calculated magnetic anomalies. The amplitude of this anomaly varies from −17 to 139 nT. The basement was

modelled by only 8 polygons. These polygons display a small range of magnetic susceptibility values ranging from 0.001 to 0.003 CGS. The low magnetic susceptibilities are associated with acidic rocks, suggesting a granitic basement of continental type. This model confirms and outlines the rough structure and composition of the basement rocks that cause the magnetic anomalies. Two drilled wells (Bahrein-1 and 2) along this transect were studied to constrain the basement depth. The depth to the basement surface determines the thickness of the sedimentary cover that ranges from 2500 to more than 5000 m. Bouguer values varies from −32 to −5mGal. The density of the modelled polygons ranges from 2.65 to 2.74 gr/cc.

Profile BB' passes through the middle part along Longitude 27°00'E and extends a distance of 165 km. The amplitude of this anomaly varies from −54 to 240 nT. The basement blocks were modelled by 10 polygons (Fig. 11). These polygons show a larger range of the magnetic susceptibility than that of the first model values, which range from 0.001 to 0.007 CGS. According to Telford et al. (1990), the magnetic susceptibilities of granitic rocks range from 0 to 0.0064 CGS, while basaltic rocks reach up to 0.014 CGS. Only the GH 22-1 well, which ended by Khatatba Formation, was utilized to constrain the basement depth. Generally, the depth to the basement surface ranges from 3000 to more than 5000 m. The gravity values change from −33 to −13mGal. The density of the modelled basement blocks ranges from 2.65 to 2.84 gr/cc.

Profile CC' (Fig. 11) is taken through the eastern part along Longitude 27°30'E and extends a distance of 165 km. The amplitude of this anomaly varies from −90 to 220 nT. The basement blocks were exhibited by 8 polygons. These polygons demonstrate a limited range of the magnetic susceptibility ranging from 0.001 to 0.005 CGS indicating granitic rocks. The depth of the basement surface reveals the shallowest basement rocks the previous profiles and ranges from 2000 to about 5000 m. The gravity anomaly has values ranging from −41 to −19mGal. The density of the modelled polygons ranges from 2.65 to 2.75 gr/cc.

Profile W E (Fig. 11d) traverses the modelled profiles AA', BB' and CC'. It covers a distance of 193 km. The amplitude of this anomaly varies from −50 to 386 nT. The basement blocks were exhibited by 10 polygons. These polygons demonstrate a limited range of the magnetic susceptibility ranging from 0.001 to 0.007 CGS indicating acidic to basic basement rocks. The depth of the basement surface ranges from 3000 to more than 5000 m. Bouguer values vary from −42 to −14 mGal. Density of the modelled polygons range from 2.65 to 2.75 gr/cc. The intersection points with other profiles have the same values for depths, susceptibilities and densities.

Table 5: The faults and trends parameters as shown by the RTP magnetic map.

WEST					Azimuth	EAST				
N	N%	L(m)	L%	L/N		L/N	L%	L(m)	N%	N
8.0	11.8	184127.7	11.7	23016.0	0:<10	19851.3	2.5	39702.7	2.9	2.0
2.0	2.9	58450.8	3.7	29225.4	10:<20	28573.9	7.2	114295.5	5.9	4.0
2.0	2.9	45475.8	2.9	22737.9	20:<30	24692.5	11.0	172847.4	10.3	7.0
1.0	1.5	19794.5	1.3	19794.5	30:<40	18861.7	6.0	94308.7	7.4	5.0
7.0	10.3	183498.9	11.6	26214.1	40:<50	23697.3	7.5	118486.6	7.4	5.0
7.0	10.3	129707.8	8.2	18529.7	50:<60	38721.1	4.9	77442.3	2.9	2.0
1.0	1.5	27333.1	1.7	27333.1	60:<70	25847.7	1.6	25847.7	1.5	1.0
3.0	4.4	53476.3	3.4	17825.4	70:<80	23646.2	4.5	70938.5	4.4	3.0
4.0	5.9	89150.0	5.7	22287.5	80:<90	18058.9	4.6	72235.4	5.9	4.0
35.0	51.5	791015.1	50.2		Sum		49.8	786104.8	48.5	33.0
∑n	68.0		∑L=1577119.9 m			∑n%	100.0		∑L%	100.0

Table 6: The faults and trends parameters as shown by the regional magnetic map.

WEST					Azimuth	EAST				
N	N%	L(m)	L%	L/N		L/N	L%	L(m)	N%	N
2.0	7.1	101214.6	9.9	50607.3	0:<10	35035.0	6.8	70070.0	7.1	2.0
1.0	3.6	51391.4	5.0	51391.4	10:<20	37523.7	7.3	75047.4	7.1	2.0
1.0	3.6	24995.4	2.4	24995.4	20:<30	27815.0	2.7	27815.0	3.6	1.0
2.0	7.1	78348.9	7.6	39174.4	30:<40	25551.1	2.5	25551.1	3.6	1.0
2.0	7.1	63989.3	6.2	31994.6	40:<50	37990.9	26.0	265936.4	25.0	7.0
0.0	0.0	0.0	0.0	–	50:<60	24020.1	4.7	48040.3	7.1	2.0
0.0	0.0	0.0	0.0	–	60:<70	31656.9	9.3	94970.8	10.7	3.0
1.0	3.6	48447.9	4.7	48447.9	70:<80	–	0.0	0.0	0.0	0.0
0.0	0.0	0.0	0.0	–	80:<90	48423.3	4.7	48423.3	3.6	1.0
9.0	32.1	368387.5	36.0		Sum		64.0	655854.2	67.9	19.0
∑n	28.0		∑L=1024241.7 m			∑n%	100.0		∑L%	100.0

Table 7: The faults and trends parameters as shown by the residual magnetic map.

WEST					Azimuth	EAST				
N	N%	L(m)	L%	L/N		L/N	L%	L(m)	N%	N
3.0	3.4	83769.7	4.8	27923.2	0:<10	17548.3	10.0	175482.6	11.4	10.0
4.0	4.5	80198.5	4.6	20049.6	10:<20	20783.4	13.0	228617.5	12.5	11.0
2.0	2.3	27101.8	1.5	13550.9	20:<30	119042.5	13.6	238084.9	12.5	2.0
4.0	4.5	65354.6	3.7	16338.6	30:<40	35592.4	8.1	142369.5	8.0	4.0
5.0	5.7	113038.8	6.4	22607.8	40:<50	24538.3	7.0	122691.5	6.8	5.0
6.0	6.8	105241.6	6.0	17540.3	50:<60	18921.3	6.5	113528.0	5.7	6.0
1.0	1.1	24434.9	1.4	24434.9	60:<70	23021.5	1.3	23021.5	1.1	1.0
5.0	5.7	74940.2	4.3	14988.0	70:<80	9004.4	2.6	45022.2	2.3	5.0
3.0	3.4	54630.9	3.1	18210.3	80:<90	12104.9	2.1	36314.6	2.3	3.0
33.0	37.5	628711.0	35.8		Sum		64.2	1125132	62.5	47.0
∑n	80.0		∑L=1753843.2 m			∑n%	100.0		∑L%	100.0

The basement structural relief map

The structural map (Fig. 12) was produced from all the pre-processed (RTP, Bouguer, Low- and high-pass, TDR) of both G/M maps. The most viewable map here is the high-pass filtered magnetic map, which gives acceptable match in most areas. Therefore, it was chosen to overlay the constructed structural relief map on it. The map shows three main highs or uplifted blocks (swells) that outline the main basins. The first one (Appolonia–Qattanyia uplift) with an ENE trend divides the Abu Gharadig Basin into northern and southern basins. The second and third uplifts with N–S and NW trends separate the Abu Gharadig Basin and the southern part of the Faghur Basin. The map shows three main basins, namely the Faghur Basin in the western part, Northern Abu Gharadig Basin (in the northern part), and the Southern Abu Gharadig Basin. The Southern Abu Gharadig Basin and Faghur basins are divided into several sub-basins (troughs) by some uplifted blocks (swells). All these sub-basins can be correlated with negative anomalies of both G/M high-pass maps. The fault pattern seems to be confined by the ENE (Syrian Arc), NE (Tibesti), N–S (East African) and NW (Suez) trends.

The resulting depths from the spectral analysis technique were plotted at the midpoint of the 21 profile. In addition, the basement surface of the 2.5D magnetic modelling was digitized from the modelled profiles (AA', BB' and CC') and plotted to contour the basement surface all over the area. The basement depth map shows depth values ranging from 1000 m in the south-western corner (stable shelf) to about 5500 m within the Faghur and Southern Abu Gharadig basins.

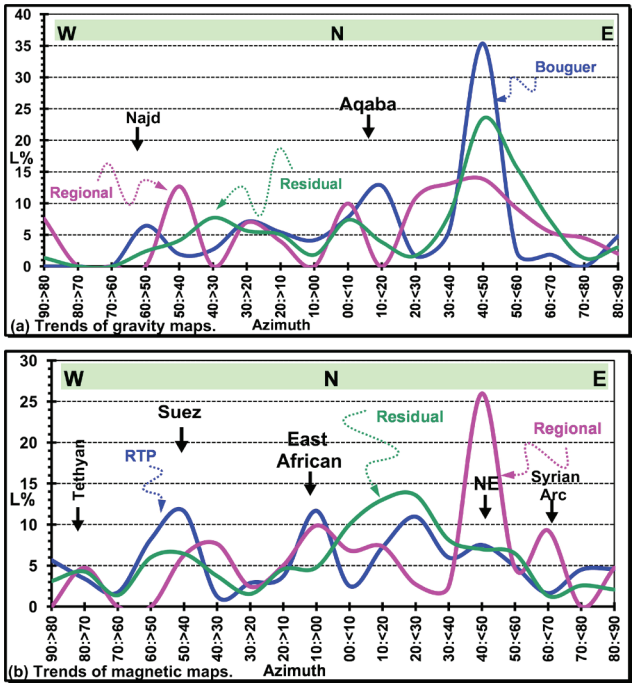

Fig. 8. The frequency curve of the deduced G/M trends shows the plot of the length percentage (L%) every 10° to the west and the east from the North.

Geothermal gradient of the area

Morgan et al. (1977) studied the geothermal gradient (GG) of the northern WD from the drilled wells. Their studies indicated that the area between latitudes 28–29°N and longitudes 25–27°E has a GG around 18.7° mK/m (=C/km). These boundaries don't cover the investigated area. In this work, it important to throw more light on the GG within the area due to its important role for maturation of the organic matter to generate hydrocarbons.

The geothermal gradient (ΔT/Δd) can be inferred from magnetic data by determining the base of magnetic sources that linked with the Curie temperature of about 580 °C. This temperature is divided by the depth to base of the magnetic source to compute the GG. A detailed methodology was described by Saada (2016).

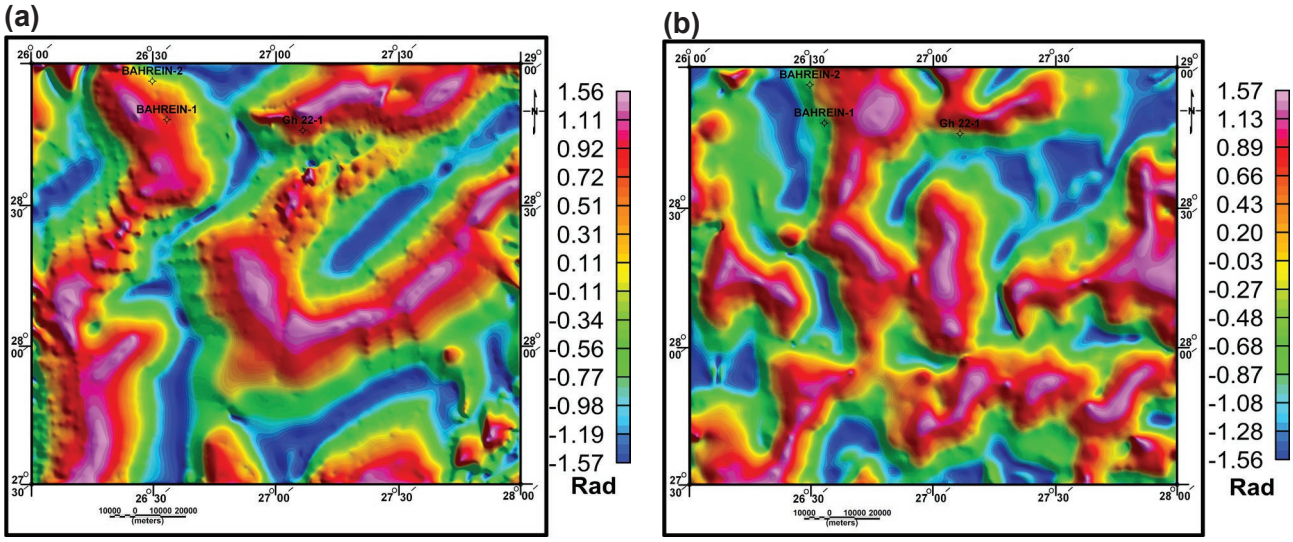

Fig. 9. a — The TDR map of the high-pass filtered gravity map. **b** — The TDR map of the high-pass filtered magnetic map.

To estimate the basal depth of magnetic source (Z_b), the effect of shallow sources and the topography must be eliminated. Therefore, the low-pass flittered magnetic map was subdivided into six areas with 100×100 km (Fig. 6b) to estimate the Z_b according to the next equation:

$$Z_b = 2Z_0 - Z_t$$

Where Z_0 represents the depth to the centroid and Z_t is the depth to the top of magnetic sources. Figure 13 displays the estimation of the GG along areas (1) and (2) as examples. Table 9 shows the results of the estimation of the GG all over the area.

The GG ranges from 18.76 to 23.15 °C/km with an average value of 20.23 °C/km. The oil window ranges from 50 to 150 °C (Howell 1993 and Sajgo 2000), which corresponds to depths of 2472 m to 7415 m. Shalaby et al. (2008) conclude that the top of the oil window in WD can be recorded at nearly 8000 ft (2438 m). They also indicate that the increasing of the maturity level deeper than 11800 ft (3596 m) that is correlated with Khatatba and older sediments exhibits a late phase of oil generation and is at the top of gas generation maturity.

As shown in Fig. 12, the thickness of the sedimentary cover exceeds 3000 m in most parts of the area. Therefore, the GG of the area is enough to generate oil from different source rocks (Fig. 2). This indicates that the area has good hydrocarbon potentialities and needs more detailed exploration within the Faghur and southern Abu Gharadig basins.

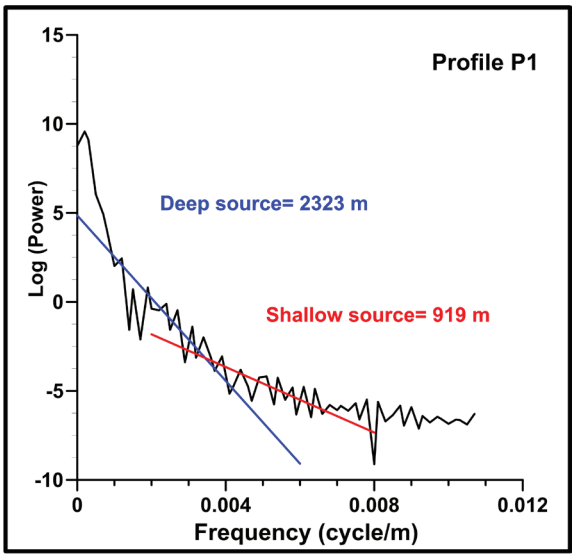

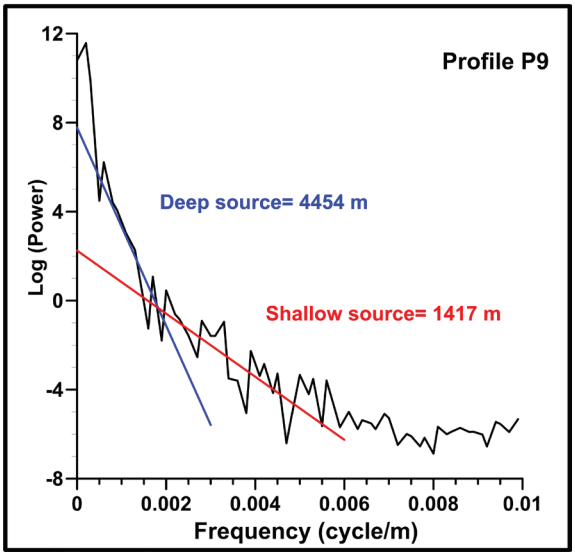

Fig. 10. Examples of spectral analysis technique along profiles P1 and P9.

Table 8: Results of spectral analysis technique.

Profile No.	Deep (m)	Shallow (m)	Profile No.	Deep (m)	Shallow (m)
P1	2323	919	**P12**	2868	813
P2	3506	1304	**P13**	2406	938
P3	3078	1002	**P14**	3597	1483
P4	3175	1113	**P15**	4116	1873
P5	3589	1134	**P16**	3828	1106
P6	3864	1551	**P17**	4012	1045
P7	3370	1412	**P18**	3541	1240
P8	2576	1117	**P19**	2947	1598
P9	4454	1417	**P20**	2796	945
P10	2841	1045	**P21**	3395	1261
P11	3219	1353			

Summary and conclusions

This work can be summarized in the following points:

- The research area lies within the unstable shelf that was affected by both folding and faulting systems except for the south-western corner.
- The stratigraphic section within the area ranges Cambro–Ordovician sediments to the Quaternary sand dunes as deduced from the drilled wells. These sediments reflect large varieties of depositional environments, which change from coarse clastics to carbonate rocks. These rocks represent the source, reservoir and cap rocks in the petroleum system in the northern WD oil province.
- The separation of regional–residual components was applied to the gravity and RTP magnetic maps, to outline the shallow anomalies from the deeper ones. The qualitative interpretation exposes a number of alternative uplifted and down-faulted blocks. The area was intruded by bodies causing high magnetic susceptibilities.
- The lineaments analysis of the Bouguer gravity and RTP magnetic maps, as well as their filtered regional and residual maps, indicate that the area was deeply affected by the tectonics of the NE (Tibesti), N–S (East African), ENE (Syrian Arc) and NW (Suez) trends.
- The TDR maps for both G/M maps detect the location and the depth of the edges/contacts within the area under consideration.
- The depth estimation to the basement rocks carried out along 21 magnetic profiles, using spectral analysis technique, shows that the depth ranges from 2332 m in the southern

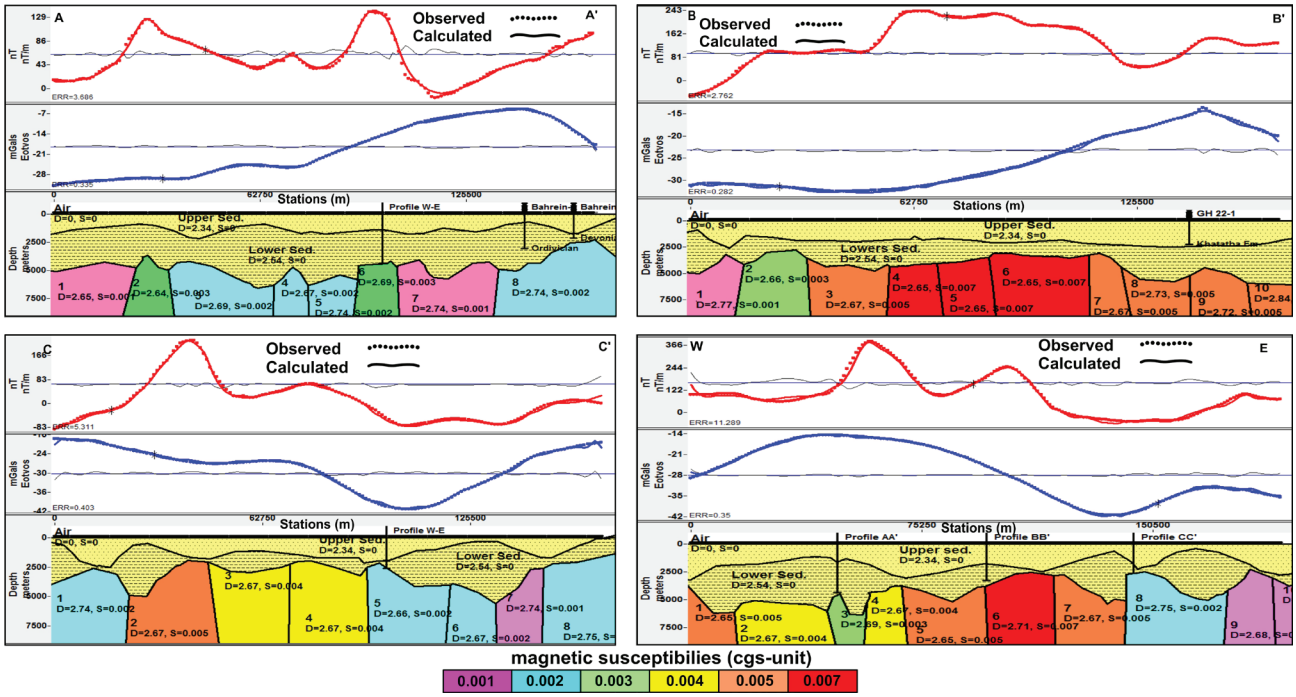

Fig. 11. The modelled profiles AA', BB' and CC'.

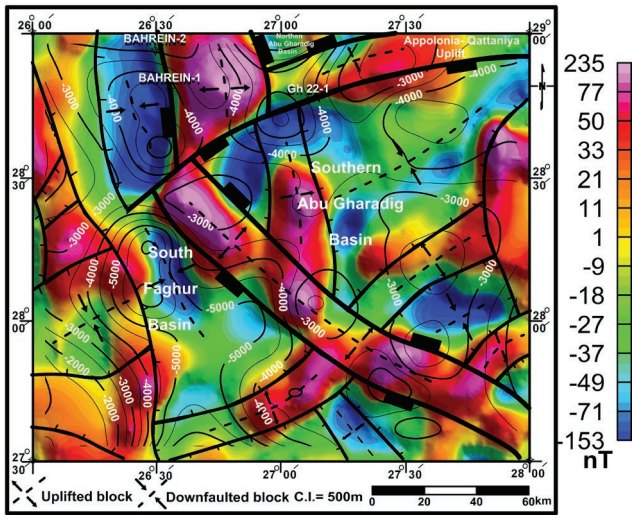

Fig. 12. Interpreted structure relief map.

parts to 4116 m and 4454 m in the central and northern parts, respectively.

- Four forward G/M models were constructed to offer additional information about the type, structure and the magnetic susceptibilities of the basement rocks. The models reveal that the sedimentary cover varies in thickness from 2000 m to about 6000 m. The basement rocks exhibit granitic rocks as deduced from the values of the magnetic susceptibilities (0.001–0.007 in CGS unit). The models indicate that the basement rock units are formed from uplifted and down-faulted blocks.
- The constructed structure relief map shows three main uplifted blocks and three basins. The first uplift (Appolonia–Qattaniya) lies on the northern part with an ENE trend and divides the Abu Gharadig Basin into the Northern and Southern Abu Gharadig basins. The second may represent an extension of the Ramak–Mubarak uplift with an N–S trend separates the Faghur Basin from the northern and southern Abu Gharadig basins. The third uplift with a NW trend outlines the southern Abu Gharadig Basin in the middle part. Smaller uplifts with ENE, N–S, and NW trends separate the southern Faghur and Abu Gharadig basins into a number of sub-basins.
- The basement relief map displays a basement depth varying from about 1000 m in the south-western corner to about 6000 m in the middle and northern parts. The map shows that the depth to the basement surface exceeds 3000 m all over the study area.
- The average geothermal gradient was estimated from magnetic data. It attains about 20.23 °C/km, which is enough to generate hydrocarbons.
- Finally, the Southern Abu Gharadig Basin represents an encouraging site for further hydrocarbon exploration. This is due to the abundance of different rock types and the thick sedimentary cover as well as a large number of faults that form uplifted and down-faulted blocks. In addition, the GG is sufficient to generate the hydrocarbons. Therefore, the area is considered as a promising site for hydrocarbon accumulations.

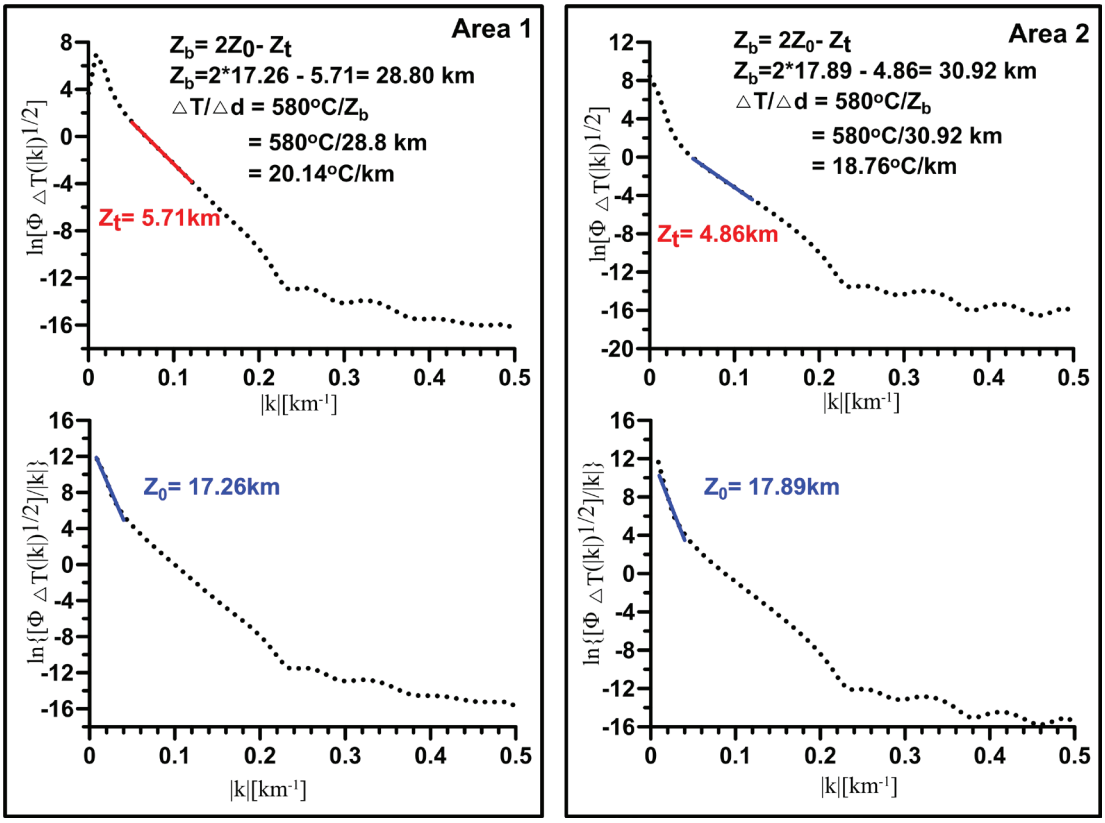

Fig. 13. Two examples of geothermal gradient (areas 1 and 2).

Table 9: The results of the estimated geothermal gradient.

Area No.	Z_0 (km)	Error Z_0	Z_t (km)	Error Z_t	Z_b (km)	$\Delta T/\Delta d$ (℃/km)
1	17.26	0.18	5.71	0.00	28.80	20.14
2	17.89	0.26	4.86	0.01	30.91	18.76
3	17.29	0.27	4.10	0.01	30.48	19.03
4	15.15	0.02	5.25	0.01	25.05	23.15
5	15.96	0.16	4.34	0.01	27.58	21.03
6	17.28	0.24	4.49	0.01	30.07	19.29
Average	16.81	0.19	4.79	0.01	28.82	20.23

Acknowledgements: The author is grateful to the Geologica Carpathica Editor Dr. Milan Kohút and three anonymous reviewers for their valuable comments and revisions that helped greatly to improve this manuscript.

References

Abdel Aal A.A. & Moustafa A.R. 1988. Structural framework in Abu El Gharadig Basin, Western Desert, Egypt. *EGPC, 9th Expl. Conf. Cairo, Egypt.*

Abdel Zaher M., Senosy M.M., Youssef M.M. & Ehara S. 2009: Thickness variation of the sedimentary cover in the South Western Desert of Egypt as deduced from Bouguer gravity and drill-hole data using neural network method. *Earth Planets Space* 61, 659–674. https://doi.org/10.1186/BF03353175

Abu El-Ata A.S. 1981: A study on the tectonics and oil potentialities of some Cretaceous–Jurssic basins, Western Desert, Egypt; using geophysical and suburface geological data. *Ph.D. Thesis, Fac. Sci. Ain Shams Univ.*

Abu El-Ata A.S., Azzam S.S., El- Khafeef A.A., Zahra H.S. & Oweis H.T. 2012: Contribution of potential field data in delineating the structural-tectonic set-up of the eastern Qattara Depression area, Western Desert, Egypt. *Australian Journal of Basic and Applied Sciences* 6, 3, 204–223.

Affleck L. 1963: Magnetic anomaly trend and spacing patterns. *Geophysics* 28, 379–395.

Azab A.A. 2014: Agnes high, Western Desert, Egypt: A structural study in view of potential data modelling. *Egypt. J. Petrol.* 23, 229–245. https://doi.org/10.1016/j.ejpe.2014.05.010

BAPETCO (Bader Petroleum Company) 2007: Generalized Litho-Stratigraphic Column of Western Desert. *Internal report*, 1–10.

Barakat M.G. 1984: General review of the petroliferous provinces of Egypt with special emphasis on their geologic setting and oil potentialities. *Petrol. and Gas Proj., Cairo Univ.* MIT Technology planning program.

Curtis C.E. & Jain S. 1975: Determination of volcanic thickness and underlying structures from aeromagnetic maps in the Silet area of Algeria. *Geophysics* 40, 79–90.

Dennis S.W. 1984: The tectonic framework of petroleum occurrence in the Western Desert of Egypt. *EGPC 7th exploration seminar Cairo.*

Dietz R.S. & Hoden J.C. 1970: Reconstraction of Pangea, break-up and dispersion of continents, Permian to present. *Journal of Geophysical Research* 75, 4939–4955.

Dolson J.C., Shann M.V., Matbouly S., Harwood C., Rashed R. & Hammouda H. 2001: The Petroleum Potential of Egypt. In: Morgan W.A.: Petroleum Provinces of the 21st Century. *American Association of Petroleum Geologists*, *Memoir* 74, 453–482.

Egyptian Geological Survey and Mining Authority 1981: Geologic map of Egypt.

El Shaarawy O.A. 1994: Structural analysis and oil potentialities of the area north of the Qattara Depression. Western Desert, Egypt, based on geophysical and subsurface geological data. *Geology Department, Ain Shams University,* Cairo, 1–196.

El-Badrawy H.T. & Soliman M.R. 2003: Subsurface evaluation of south Kharga Oasis area, south Western Desert, Egypt. *Egyptian Geophysical Society Journal* 1, 1, 31–41.

El-Gezeery M. 2006: Crustal thickness and structure of the northwestern part of the western desert, as deduced from integrated gravity and deep seismic data. *Egyptian Geophysical Society Journal* 4, 1, 77–88.

El-Kenawy A.A. 2000: Interpretation of potential field data of the area between latitudes 27°30'–29°00'N and longitudes 26°00'E, Western Desert, Egypt. *Ph.D. Thesis, Fac. Sci. Zagazig Univ.*

El-Khadragy A.A., Saad M.H. & Azab A. 2010: Crustal Modeling of South Sitra Area, North Western Desert, Egypt Using Bouguer Gravity Data. *Journal of Applied Sciences Research* 6, 1, 22–37.

Fairhead J.D., Salem A., Williams S. & Samson E. 2008: Magnetic interpretation made easy: The tilt-depth-dip-Dk method. In: 2008 annual international meeting expanded abstracts. *Society of Exploration Geophysicists*, 779–783.

General Petroleum Company (GPC) 1984: Bouguer gravity map of Egypt.

Geosoft Oasis Montaj Program 2007: Geosoft Mapping and Application System, standard edition, version 6.4.2 (HJ*), Geosoft Inc*.

Gulf of Suez Petroleum Company (GUPCO) 1994: A high sensitivity aeromagnetic survey of Egypt.

Hinze W.J., Von Frese R.R.B. & Saad A.H. 2013: Gravity and magnetic exploration: Principles, practices, and applications. *Cambridge University Press,* New York, 1–525.

Howell D.G. 1993: The future of energy gases. *U.S. Geological Survey*, 1–890. https://doi.org/10.3133/pp1570

Maden N., Aydin A. & Kadirov F. 2015: Determination of the Crustal and Thermal Structure of the Erzurum-Horasan-Pasinler Basins (Eastern Turkiye) Using Gravity and Magnetic Data. *Pure Appl. Geophys*. 172, 1599–1614. https://doi.org/10.1007/s00024-014-1001-x

Meshref W.M. 1982: Regional structure setting of the Northern Egypt. *EGPC, 6th Exploration Seminar, Cairo, Egypt.*

Meshref W.M. 1990: Tectonic framework. In: Said R. (Ed.): The geology of Egypt. *A.A. Balkema Publishers*, Rotterdam, 113–130.

Meshref W.M. 1995: Well evaluation conference of Egypt. *Schlumberger Technical Editing Services, EGPC, Egypt*, 1–87.

Meshref W.M. 2002: Basement tectonic map of Egypt. *Cairo international petroleum conference and inhabitation, Cairo,* 1–5.

Miller H.G. & Singh V. 1994: Potential field tilt – a new concept for location of potential field sources. *Journal of Applied Geophysics* 32, 213–217.

Mohamed A.K., Ghazala H.H. & Mohamed L. 2016: Integration between well logging and seismic reflection techniques for structural analysis and reservoir characterizations, Abu El Gharadig basin, Egypt. *NRIAG Journal of Astronomy and Geophysics* 5, 362–379. https://doi.org/10.1016/j.nrjag.2016.07.003

Morgan P., Blackwell D.D., Farris J.C., Boulos F.K. & Salib P.G. 1977: Preliminary geothermal gradient and heat flow values for northern Egypt and the Gulf of Suez from oil well data. In: Proceedings, Int. Cong. Thermal Waters, geothermal Energy and Volcanism of the Mediterranean Area. *Nat. Tech. Univ.,* Athens, 1, 424–438.

Naidu P.S. 1970: Statistical structure of aeromagnetic field. *Geophysics* 35, 279–292.

Nettleton L.L. 1976: Gravity and magnetics in oil prospecting. *Mc-Graw-Hill Book Co. Inc.,* New York, 1–464.

Rama Rao Ch., Kishore R.K., Pradeep Kumar V. & Butchi Babu B. 2011: Delineation of intra crustal horizon in Eastern Dharwar Craton – an aeromagnetic evidence. *J. Asian Earth Sci.* 40, 534–541. https://doi.org/10.1016/j.jseaes.2010.10.006

Reddi A.G.B., Mathew M.P., Baldau S. & Naidu P.S. 1988: Aeromagnetic evidence of crustal structure in the granulite terrane of Tamil Nadu–Kerala. *J. Geol. Soc. India* 32, 368–381.

Saada S.A. 2016: Curie point depth and heat flow from spectral analysis of aeromagnetic data over the northern part of Western Desert, Egypt. *Journal of Applied Geophysics*, 134, 100-111. https://doi.org/10.1016/j.jappgeo.2016.09.003

Saada S.A. & El-Khadragy A.A. 2015: An Integrated Study of Gravity and Magnetic Data on West El-Minya Area, Western Desert, Egypt. *Journal of American Science* 11, 12, 169–184. https://doi.org/10.7537/marsjas111215.23

Said R. 1962: The Geology of Egypt. *Elsevier*, Amsterdam, 1–377.

Said R. 1990: The Geology of Egypt. *Bakema*, Rotterdam, 1–734.

Sajgo Cs. 2000: Assessment of generation temperatures of crude oils. *Organic Geochemistry* 31, 1301–1323. https://doi.org/10.1016/S0146-6380(00)00097-8

Salem A., Williams S., Fairhead J., Ravat D. & Smith R. 2007: Tilt depth method: a simple depth estimation method using first-order magnetic derivatives. *Lead Edge* 26,1502–1505. https://doi.org/10.1190/1.2821934

Salem A., Williams S., Fairhead D., Smith R. & Ravat D. 2008: Interpretation of magnetic data using tilt-angle derivatives. *Geophysics* 73, L1–L10. https://doi.org/10.1190/1.2799992

Selim E. & Aboud E. 2012: Determination of sedimentary cover and structural trends in the Central Sinai area using gravity and magnetic data analysis. *J. Asian Earth Sci.* 43, 193–206. https://doi.org/10.1016/j.jseaes.2011.09.010

Shaaban Fa., Shaaban Fo. & Ibrahim S. 2012: Reflection Seismic studies on the Razzak oil field, Western Desert, Egypt. *Nature and Science* 10, 3, 7–15.

Shahin A.N. 1989: Undiscovered reserves in the Northern Western Desert, Egypt: Application of Quantitative Modelling to Petroleum Exploration. In: Proc. 28th Int. Geol. Cong., Washington, D.C 3, 3–82.

Shahin A.N. & Al-Awadly A.M. 2011: Petroleum Systems in the North Western Desert of Egypt. *Life Science Journal* 8, 2, 676–685.

Shalaby M.R., Abdullah W.H. & Abu Shady A.N. 2008: Burial history, basin modeling and petroleum source potential in the Western Desert, Egypt. *Bulletin of the Geological Society of Malaysia* 54, 103–113. https://doi.org/10.7186/bgsm2008017

Spector A. & Grant F.S. 1970: Statistical models for interpreting aeromagnetic data. *Geophysics* 35, 293–302.

Sultan N. & Abdel Halim M. 1988: Tectonic framework of northern Western Desert, Egypt and its effect on hydrocarbon accumulations. *9th EGPC Expl. Conf. CONOCO*.

Telford W.M, Geldart L.P. & Sheriff R.E. 1990: Applied geophysics. 2nd ed., Cambridge Univ. Press, *Cambridge*. https://doi.org/10.1017/CBO9781139167932

Thébault E., Purucker M., Kathryn A., Langlais W.B. & Sabaka T.J. 2010: The magnetic field of the earth's lithosphere. *Space Sci. Rev.* 155, 95–127. https://doi.org/10.1007/s11214-010-9667-6

Troshkov G. A. & Shalaev S.A. 1961: Application of the Fourier transform to the solution of the reverse problem of gravity and magnetic survey. *Preh. Geofiz* 30, 162–178.

Verduzco B., Fairhead J.D., Green C.M. & MacKenzie C. 2004: New insights into magnetic derivatives for structural mapping. *Lead Edge* 23,116–119. https://doi.org/10.1190/1.1651454

Youssef M.I. 1968: Structural pattern of Egypt and its interrelation. *American. Assoc. Petrol. Geol. Bull.* 52, 4, 601–614.

Youssef M.M. 2003: Structural setting of central and south Egypt: An overview. *Micropaleontology* 49, Suppl. 1, 1–13.